1   **Flow-Substrate Interactions in Aggrading and Degrading Submarine Channels**

2   **Anjali M. Fernandes[1,2], James Buttles[1], David Mohrig[1], Kyle M. Straub[3]**

3   *[1]The Center for Integrative Geoscience, University of Connecticut, Storrs, Connecticut, USA.*

4   *[2]The Jackson School of Geosciences, The University of Texas at Austin, Texas, USA.*

5   *[3]Department of Earth and Environmental Sciences, Tulane University, 6823 St. Charles Avenue, New*

6   *Orleans, Louisiana 70118-5698, USA*

7   *Email: anjali.fernandes@uconn.edu*

8   Keywords: Turbidity currents; submarine channels; submarine canyons; boundary layer roughness; flow-

9   separation zones; erosional bedforms; detachment-limited channels; transport-limited channels; Shields

10   scaling

11   **ABSTRACT**

12   Connecting real time measurements of current-bed interactions to the temporal evolution of

13   submarine channels can be extremely challenging in natural settings. We present a suite of physical

14   experiments that offer insight into the spectrum of interactions between turbidity currents and their

15   channels, from (i) detachment-limited erosion to (ii) transport-limited erosion to (iii) pure deposition. In

16   all three cases channel sinuosity influenced patterns of erosion and deposition; the outsides of bends

17   displayed the highest erosion rates in the first two cases, whereas the outsides of bends were associated

18   with the highest deposition rates the third. We connect the evolution of these channels to the turbulence of

19   the near-bed boundary layer. In the erosional experiments both channel beds roughened through time,

20   developing erosional bedforms or trains of ripples. Reynolds estimates of boundary layer roughness

21   indicate that, in both erosional cases, the near-bed boundary layer roughened from smooth or

22   transitionally rough to rough, whereas the depositional channel appears to have remained consistently

23   smooth. Our results suggest that, in the absence of any changes from upstream, erosion in submarine

24   channels is a self-reinforcing mechanism whereby developing bed roughness increases turbulence at the

25   boundary layer, thereby inhibiting deposition, promoting sediment entrainment and enhancing channel

26   relief; deposition occurs in submarine channels when the boundary layer remains smooth, promoting

27   aggradation and loss of channel relief.

28   **INTRODUCTION**

29   Continental margins are patterned with channels and canyons that convey large volumes of

30   sediment to the deep ocean. These channels evolve through erosion and/or deposition, often aggrading

31   over significant vertical distances (Pirmez et al., 2000), or by carving canyons (Babonneau et al., 2010;

32   Conway et al., 2012) many hundreds of meters deep. Physical experiments can offer insight into current-

33   bed interactions. Such measurements are challenging to acquire in natural settings and even more

34   challenging to relate to the temporal evolution of submarine channels (Khripounoff et al., 2003; Xu et al.,

35   2004, 2013; Xu, 2010; Hughes Clarke, 2016; Symons et al., 2017; Azpiroz-Zabala et al., 2017b, 2017a).

36   In the past, some experiments e.g. (Mohrig and Buttles, 2007; Straub et al., 2008; Janocko et al., 2013)

37   focused on purely depositional turbidity currents that were suspension-dominated, whereas others

38   investigated erosional currents that modified channels primarily through bedload-transport (Métivier et

39   al., 2005; Amos et al., 2010). Here we present three experiments which we use to explore the processes

40   that shape submarine channels, along the continuum of intensely erosional to purely depositional in

41   connection to the hydraulic characteristics of the near-bed boundary layer, across this spectrum of

42   behaviour.

43   **Detachment-limited and transport-limited erosion in terrestrial landscapes**

44   Terrestrial channels eroding into bedrock have been modeled using: a) a detachment-limited model

45   in which the resistance of the substrate is the limiting factor that controls the erosion rate, and b) a transport-

46   limited model where the erosion rate is limited by the ability to transport the eroded sediment (Howard,

47   1980, 1994; Whipple, 2004). Detachment-limited erosion is more sensitive to local conditions (e.g.

48   topographic or bed roughness) rather than reach-averaged conditions (e.g. discharge; (Johnson and

49   Whipple, 2007). Erosion generally takes place through abrasion and wear by the impacts of sediment being

50   transported by the flow, and turbulence generated by evolving bed roughness. These channels are

51   characterized by knickpoints, inner channels, scour holes, grooves, and sculpted bedforms (Whipple, 2004).

52   The transporting currents are efficient at removing sediment in transport from upstream and at entraining

53   material from the local substrate.

54   When the removal of eroded sediment is not efficient, sediment is stored in patches on the bed,

55   protecting the bed from further erosion in a phenomenon referred to as the 'cover-effect' (Johnson et al.,

56   2009). Erosional channels with abundant sediment cover on the channel bed are referred to as "transport-

57   limited" (Shepherd and Schumm, 1974; Sklar and Dietrich, 2004; Whipple, 2004; Johnson and Whipple,

58   2007). Partially-alluviated erosional channels scouring into compact, indurated sediment have been

59   observed in depositional landscapes such as the Mississippi River Delta (Edmonds et al., 2011; Nittrouer

60   et al., 2011a), where cover effects are particularly evident. Channel bottoms display deep scours where they

61   are devoid of alluvial cover at the outsides of river bends. All natural erosional channels can be expected to

62   display some combination of detachment-limited and transport-limited behaviour (Whipple, 2004). Here

63   we use 2 experiments to study the characteristics of detachment-limited and transport-limited erosion in

64   submarine channels. For completeness, we incorporate data from an aggradational channel experiment

65   (Straub et al., 2008). We use these experiments to explore the role of the near-bed boundary layer in the

66   spectrum of forms and deposit characteristics observed.

67   **<u>Dynamic scaling of experiments to natural systems</u>**

68   Laboratory experiments have historically been compared to natural systems by using three

69   dimensionless variables: (1) the densimetric Froude number (Fr_d), (2) the Reynolds number (Re), and (3)

70   the ratio of current shear velocity u* to particle fall velocity w_s (Middleton, 1966; Baas et al., 2004; Yu et

71   al., 2006; Mohrig and Buttles, 2007; Straub et al., 2008; Amos et al., 2010; Rowland et al., 2010; Cantelli

72   et al., 2011). The first parameter, the Froude number, defines the ratio between momentum and

73   gravitational forces within the transporting current and is traditionally maintained equal or similar to

74   natural analogues. The Reynolds number, which quantifies the turbulence of the currents, cannot be equal

75   to natural flows in scaled-down laboratory settings. The third parameter, also referred to as a Shield's

76   parameter (Shields, 1936; Bagnold, 1966; Smith and Hopkins, 1971; van Rijn Leo C., 1984; Nino et al.,

77   2003), characterizes how sediment is transported. Flows in which the turbulent shear, expressed as the

78   shear velocity u*, is significantly larger than the gravitational settling velocity w_s will be more competent

79   at transporting sediment in suspension over significant distances (Shields, 1936; Smith and Hopkins,

80   1971) and will prelude sediment-bed interactions over short length scales; if u* is comparable to w_s,

81   sediment can be transported as either saltating or incipiently suspended load, dependent upon the intensity

82   of turbulence associated with current-bed interactions. In channelized turbidity currents, the intensity of

83   near-bed turbulence is the combined result of turbulent eddies shed at the scale of individual particles (de

84   Leeuw et al., 2016), of bed roughness (e.g. bedforms, scours, etc.) (Eggenhuisen et al., 2010;

85   Eggenhuisen and McCaffrey, 2012; Arfaie et al., 2018), as well as of planform irregularities (e.g. curved

86   channels) (Straub et al., 2011) which can impart turbulent shear from non-uniform spatial accelerations.

87   The magnitude of turbulence will scale with the magnitudes of fluid shear (u*) and the size of the element

88   under consideration (e.g. particle diameter, dune height, scour depth, bend amplitude, etc.). Turbulence

89   associated with these roughness scales contributes to entrainment of sediment from the bed and walls of

90   channels, and encourages vertical mixing which maintains sediment in suspension. The ratio between

91   fluid shear and the viscous forces which act to damp turbulence can be used to characterize the roughness

92   of the near-bed boundary layer (Garcia, 2008).

93   De Leeuw et al. (2016) argued that realistic turbulence-sediment interactions were critical for

94   effectively modelling submarine channel inception and evolution, and proposed a scaling approach defined

95   by the ratio of the Shield's parameter to the particle Reynolds number (Re_p). In this scaling approach, the

96   Shield's parameter is held similar between experimental and naturally occurring density currents, but the

97   similarity between the particle Reynolds numbers is relaxed as long as the boundary layer is rough or

98   transitionally rough (Garcia, 2008; de Leeuw et al., 2016). Leeuw et al. (2017) noted that density currents

99   in most previous experiments were highly depositional because the boundary layers were hydraulically

100   smooth and/or the Shields parameter fell below the initiation of suspension.

101   In Figure 1, we adopt the Shield's scaling proposed by de Leeuw et al. (2016) to compare flow and

102   sediment transport characteristics of the three experiments presented here to past experimental and field

103   measurements. Although the shear stresses associated with all three experiments exceeded the threshold for

104   the initiation of suspension, they straddle the threshold between hydraulically smooth and transitionally

105   rough boundary layers. Furthermore, Experiments 1 and 2 scale best with recent field observations of flow

106   and transport in natural systems. Using sediment with much lower densities than silica in these experiments

107   allowed us to use sand-sized particles that had transitionally rough boundary layers and high Shields

108   parameters, and were therefore easy to suspend and maintain in suspension.

109   **Experiment Design**

110   In each experiment, calcium chloride salt and water (and sediment, when it was used), were mixed

111   together in a reservoir, until the salt was completely dissolved. The mixture was agitated over several hours

112   and allowed to cool to room temperature, as the dissolution of this salt in water is an exothermic process.

113   Once at room temperature, the mixture was pumped up to a constant head tank and then allowed to flow

114   into the experimental basin at a controlled rate set by the constant hydraulic head and a system of valves.

115   The two experimental basins were designed along similar lines, shown by the generalized schematic in

116   Figure 2. In all experiments, density currents were released into an experimental channel through a box

117   with two perforated screens designed to extract momentum from flows. The pre-formed channels were built

118   upon a platform separated from the walls of the basin by deep moats that prevented currents from reflecting

119   off the basin walls. Saline fluid was not allowed to collect in the basin and was extracted through the floor

120   drains as it flowed off the raised platform. The water level in the basin was maintained with a constant flux

121   of fresh water and overflow drainage through a weir. The basin used in Experiment 1 was 8 m long, 6 m

122   wide and 2 m deep. The basin used for Experiments 2 & 3 was 5 m long, 4.5 m wide and 0.8 m deep. In all

123   experiments, the channel was constructed diagonally across the false floor.

124   The channels used in these experiments were designed with similar sinuosity, but different

125   sediment and flow properties (Table 1). In Experiment 1, the channel was built entirely out of a weakly

126   cohesive mixture of acrylic particles (specific gravity = 1.15) and clay positioned on top of a sloping ramp.

127   The sediment was mixed in a 10:1 volumetric ratio. The first two currents released into the channel were

128   saline density currents (excess density = 4%). These were followed by three more density currents that

129   carried a 2% volumetric concentration of suspended acrylic sediment.

130   In Experiment 2 a saline density current (excess density = 3.32%) was released through the

131   experimental channel which consisted of a cohesionless, 2-cm thick bed of acrylic particles draped over a

132   sinuous channel form built from concrete. In Experiment 3 sixteen purely depositional currents flowed

133   through a channel constructed of concrete with a thin layer of silica sediment on the bed. Currents had an

134   excess density of 2.1%. 33% of this excess density was supplied by suspended sediment in the current, and

135   the remaining 67% was from dissolved salt. High-resolution bathymetry maps (horizontal resolution =

136   4mm; vertical resolution ~100 microns for Experiments 1 & 2; ~1mm for Experiment 3), collected before

137   and after each flow defined patterns of bed change for all three cases. Key geometric and dynamic properties

138   of the experimental designs are compiled in Table 1.

139   **Table 1: Summary of geometric and dynamic properties of Experiments 1, 2 and 3.**

	Parameter	Experiment 1	Experiment 2	Experiment 3
Channel geometry	Channel depth (m)	0.15	0.09	0.11
	Channel width (m)	0.50	0.40	0.40
	Down-channel slopes (degrees)	7.00	2.00	1.00
	Initial mean thickness of erodible bed (m)	0.07	0.02	0.00
	Channel sinuosity	1.15	1.28	1.28
Sediment properties	Sediment density (ρ_s) (kg/m^3)	1150.00	1150.00	2650.00
	D_1	49	49	1.7
	D_{10}	88	88	12.9
	D_{25}	127	127	23
	D_{50}	146	146	31
	D_{75}	205	205	41
	D_{90}	243	243	52.1
	D_{99}	340	340	80
Flow properties	Flow thickness (m)	0.10	0.09	0.10
	Current density (ρ_f) (kg/m^3)	1040	1033.20	1021
	Depth-averaged downstream velocity (u) (m/s)	0.10	0.05	0.08
	Shear velocity (u*) (m/s)	0.04	0.03	0.04
	Froude number (Fr)	0.50	0.26	0.56
	Reynolds number (Re)	10000.00	4050.00	8000.00

Particle Reynolds number (Re_p)	6.53	4.38	1.24
Shields parameter	13.20	5.56	3.30
Bed roughness scale (H_{bed}) (m)	0.01 - 0.05	0.01 - 0.02	-
Reynolds number from bed roughness (Re_{bed})	~650 - 2236	~330- 660	-

140

Results

142   Integrating surface change for each flow in all three cases reveal net erosion in Experiments 1 and

143   2, and net deposition in Experiment 3.

Experiment 1

145   In Experiment 1, all 5 currents released through the channel modified it through net erosion (Fig.

146   3 A, Fig. 4). The weakly cohesive bed consisted of sediment that was easily suspended once it detached

147   from the surface (Fig. 1). Extreme run-up of currents onto the outer walls of channel bends occurred,

148   resulting in the formation of a low-velocity flow-separation zone (depth-averaged velocity ~= 1-2 m/s) at

149   the inner bank (Fig. 4G; Fig.5) (Leeder and Bridges, 1975; Fernandes et al., 2018). Erosion occurred

150   beneath the pathway of the high-velocity (depth-averaged velocity = 10m/s) core of the current, which

151   travelled along the outside of bends and created a series of discontinuous scours. Initially, while the channel

152   bed was smooth, the most intense scouring occurred at the outside of bends (Fig. 4A, B, H; Fig. 6).

153   Subsequently, the rough edges of scours became sites of focussed erosion (Fig. 4C-F, I-L; Fig. 6A-C) and

154   resultant elongation of scours resulted in the formation of a discontinuous inner channel (Fig. 7A- B).

155   Focussed erosion at the downstream edges of scours released clouds of suspended sediment that were

156   transported downstream and out of the system. Consecutive inner bank areas were separated by a swath of

157   erosion, and evolved into raised terraces within the low-velocity flow separation zone (Fig. 3A, Fig. 4;

158   (Fernandes et al., 2018). The channel bed evolved from smooth to ornamented, displaying erosional

159   bedforms with centimeter-scale relief (Fig. 3A; Fig. 6). These bed morphologies are similar to those

160   observed in detachment-limited terrestrial channels, where erosion is limited by the strength of the substrate

161   and bed erosion occurs primarily through wear by abrasion and plucking (Whipple et al., 2000; Whipple,

162   2004). The channel remained net-erosional through its entire length (Fig. 3A; Fig. 4).

163   **Experiment 2**

164   This channel was modified through net-erosion, with a fraction of mobilized sediment leaving the

165   system in suspension while the remainder was reworked into a continuous train of bedforms (Fig. 3B). As

166   in Experiment 1, the high velocity core of the density current travelled along the outsides of bends, resulting

167   in: 1) erosion of sediment at the outer bank, where sediment removal exposed the underlying erosion-

168   resistant channel form in the troughs between sediment-starved bedforms, and 2) deposition at the inner

169   bank, which resulted from the convergence of downstream and cross-stream bedload transport (Fig. 3B,

170   Fig 7C-D). These zones of deposition began just upstream from the points of maximum channel curvature,

171   and were connected across inflection points through the continuous bedform field (Fig. 4B). Erosion in this

172   experiment was less efficient than in Experiment 1. Abundant sediment cover on the channel bed is

173   suggestive of erosional mechanics similar to that of transport-limited erosional terrestrial channels, which

174   are also characterized by alluviated channel beds interrupted by variable degrees of local scouring

175   (Whipple, 2004; Nittrouer et al., 2011a, 2011b), and in which the erosion rate is limited by the ability of

176   the flow to transport the eroded sediment.

177   **Experiment 3**

178   Currents modified this channel via net sediment deposition (Straub et al., 2008). The thickest

179   deposition closely tracked the pathway of the high velocity core, which was inferred to be the pathway of

180   the highest suspended sediment concentration (Fig. 9 of Straub et al., 2008). This resulted in thicker deposits

181   at the outer banks of bends and thinner deposits in low-velocity zones at the inner banks of bends (Fig. 3C,

182   Fig. 7E-F). Deposits from each current draped the entire channel (Fig. 7E-F), and thinned in the downstream

183   direction (Fig. 6D-F). Sediment was primarily transported as and deposited from suspended load.

184   Suspended sediment flux was estimated to be roughly 40 times that of bedload flux (Straub et al., 2008).

185   **<u>Discussion</u>**

186   **<u>Boundary layer roughness in erosional and depositional channels</u>**

187   The transporting currents in all three experiments had shear stresses that were high enough to

188   transport sediment in suspension. Yet their temporal evolution spanned the spectrum from intense erosion

189   to pure deposition. In all three cases, planform irregularity influenced the spatial variability in sedimentation

190   and/or erosion by influencing the path of the highest velocities and sediment concentrations. A key

191   difference between the 3 experiments lies in the characteristics of the hydraulic boundary layer and the

192   temporal evolution of the three channels suggests strong agreement with the Shield-scaling predictions of

193   de Leeuw et al., 2016. Particle-scale Reynolds estimates of boundary layer turbulence place Experiment 1

194   in the transitionally rough hydraulic regime, whereas Experiment 2 was at the approximate boundary

195   between the smooth and transitionally rough regime, and Experiment 3 was squarely within the

196   hydraulically smooth regime. Furthermore, Experiment 1 evolved from a smooth bed to one patterned by

197   scours, grooves and other centimeter-scale erosional bedforms; Experiment 2 evolved from a smooth bed

198   into a semi continuous bedform field. In both erosional experiments the roughening of the channel bed is

199   likely to have encouraged greater turbulence at the near-bed boundary (Fig. 2).

200   At the start of Experiment 1, the smooth sediment bed was modified by erosion along the pathway

201   of the high velocity core; the magnitude of erosion appeared to be greatest near the outsides of bends (Fig.

202   4A, B, G, H). Particle Reynolds numbers calculated from mean, depth-averaged downstream velocities at

203   the outsides (0.1 m/s) and insides (0.01 - 0.02 m/s) of bends point to a hydraulically smooth boundary layer

204   within the flow separation zone at the inside of the bend, and a transitionally rough boundary layer at the

205   outside (Fig. 2). The emergence of erosional roughness with 1-5 centimeter relief is likely to have further

206   roughened the boundary layer, prohibiting sediment deposition and increasing erosion at sites with

207   enhanced roughness (Fig. 3A; Fig. 4; Fig.6). Near bed turbulence increased by at least two orders of

208   magnitude (Re_{bed} ~450 for 1cm relief; Re_{bed} ~ 2200 for 5cm relief; Fig. 2), causing a regime shift towards

209   a hydraulically rough boundary layer (Garcia, 2008). Hydraulically smooth boundary layers in flow

210   separation zones at the inner banks (Fig. 2) precluded erosion and very low suspended sediment fluxes were

211   unfavourable for deposition. Overall, Experiment 1 evolved in such a way that sediment entrainment and

9

212   removal remained efficient through time, and channel relief consistently increased as currents scoured into

213   the ~7cm thick erodible sediment bed (Fig. 6A; Fig 7A). Detachment-limited erosion is indicated by

214   evolution of sculpted erosional bedforms, efficient sediment removal and enhanced erosion linked to local

215   bed roughness. The temporal evolution of this channel therefore offers significant insights into the evolution

216   of topography and flow-bed interactions in detachment-limited erosional submarine channels and canyons

217   e.g. (Conway et al., 2012; Vachtman et al., 2013; Mitchell, 2014) that incise into compacted or indurated

218   fine-grained sediment on the upper continental slope and are efficient, dominantly-erosional conduits for

219   sediment transport into the deep ocean.

220   Like Experiment 1, Experiment 2 also evolved from a smooth bed to a rough one and the outer

221   banks of bends were sites of enhanced erosion. Using ripple crest height of 1-2 cm as the relevant length

222   scale, Reynolds estimates indicate that the boundary layer evolved to become hydraulically rough (Fig. 2;

223   (Garcia, 2008), though it was at the threshold between hydraulically smooth and transitionally rough at the

224   start of the experiment (Table 1). The Shields parameter for all particle sizes present falls above the

225   threshold for initiation of suspension (Shields, 1936; Bagnold, 1966; Smith and Hopkins, 1971; van Rijn

226   Leo C., 1984; Nino et al., 2003), suggesting that the rate of erosion was limited by the currents' capacity to

227   transport the sediment in suspension, and that the sediment that could not be suspended was transported as

228   bedload. The development of a bedform field, while it likely facilitated sediment entrainment by roughening

229   the boundary layer probably also reduced fluid momentum and the capacity of the current to suspend

230   sediment. This style of transport-limited erosion (Whipple, 2004; Johnson and Whipple, 2007) likely offers

231   insight into the delicate balance of flow-sediment feed-backs that control spatially variable sedimentation

232   and erosion in dominantly bypassing submarine channels on the middle or lower continental slope.

233   Unlike Experiments 1 and 2, Experiment 3 remained depositional for the duration of the

234   experiment. Straub et al., (2008) noted that super-critically climbing ripples were present over only

235   approximately 5% of the sediment bed. Consistent deposition and reduction in channel relief (Straub et al.,

236   2008)   through time suggests that the boundary layer characteristics likely shifted further into the

237   hydraulically smooth regime. We suggest that this style of evolution would be most characteristic of

238   channels near the terminus of submarine transport systems, on terminal lobes on the basin flow where

239   sediment is delivered by depletive flows that are unable to re-entrain sediment.

240   **CONCLUSIONS**

241   It is extremely challenging to connect current-bed interactions to the temporal evolution of

242   submarine channels in natural settings (Khripounoff et al., 2003; Xu et al., 2004, 2013; Xu, 2010; Hughes

243   Clarke, 2016; Symons et al., 2017; Azpiroz-Zabala et al., 2017b, 2017a). We used 3 experiments in which

244   we relate near bed turbulence, as a function of evolving bed roughness, to patterns of erosion and

245   deposition. In all three experiments presented here, channel sinuosity influenced patterns of erosion and

246   deposition. Although the currents used in all three case displayed shear stresses high enough to suspended

247   sediment, the temporal evolution in the turbulence near-bed boundary layer was also very important in

248   deciding whether the channel evolved through erosion or deposition. In the experiments where the

249   boundary layer was transitionally rough the channel evolved through erosion, developing a roughened

250   bed. In both cases, the near-bed boundary layer roughened from smooth or transitionally rough to rough,

251   enhancing near-bed turbulence. When the channel substrate was cohesive, the channel bed evolved

252   through detachment-limited erosion and most of the sediment left the system in suspension. The channel

253   bed was patterned by erosional bedforms, grooves, inner-bank terraces and a semi-continuous inner

254   channels. When the sediment was non-cohesive, the erosion was limited by the ability of the currents to

255   transport sediment and the channel bed evolved into trains of ripples. In contrast, the channel with a

256   hydraulically smooth boundary layer evolved through consistent deposition and the boundary layer

257   appears to have remained hydraulically smooth. To our knowledge, this work presents the first instance in

258   which detachment-limited erosional channels with realistic sediment transport patterns and sediment-

259   turbulence interactions have been designed successfully in laboratory settings. Our results suggest that

260   erosion in submarine channels is a self-reinforcing mechanism whereby developing bed roughness

261   increases turbulence at the boundary layer, enhancing erosion and inhibiting deposition; deposition in

262 submarine channels occurs if the boundary layer is smooth, promoting channel aggradation and loss of

263 channel relief.

Acknowledgements

References cited

268 Alexander, J., McLelland, S.J., Gray, T.E., Vincent, C.E., Leeder, M.R., and Ellett, S., 2007, Laboratory
269   sustained turbidity currents form elongate ridges at channel mouths: Channel mouth deposition from
270   sustained turbidity currents: Sedimentology, v. 55, p. 845–868, doi:10.1111/j.1365-
271   3091.2007.00923.x.

272 Amos, K.J., Peakall, J., Bradbury, P.W., Roberts, M., Keevil, G., and Gupta, S., 2010, The influence of
273   bend amplitude and planform morphology on flow and sedimentation in submarine channels: Marine
274   and Petroleum Geology, v. 27, p. 1431–1447, doi:10.1016/j.marpetgeo.2010.05.004.

275 Arfaie, A., Burns, A.D., Dorrell, R.M., Ingham, D.B., Eggenhuisen, J.T., and McCaffrey, W.D., 2018,
276   Optimisation of flow resistance and turbulent mixing over bed forms: Environmental Modelling &
277   Software, v. 107, p. 141–147, doi:10.1016/j.envsoft.2018.06.002.

278 Azpiroz-Zabala, M., Cartigny, M.J.B., Sumner, E.J., Clare, M.A., Talling, P.J., Parsons, D.R., and
279   Cooper, C., 2017a, A General Model for the Helical Structure of Geophysical Flows in Channel
280   Bends: General model for helical flows in bends: Geophysical research letters, v. 44, p. 11,932–
281   11,941, doi:10.1002/2017GL075721.

282 Azpiroz-Zabala, M., Cartigny, M.J.B., Talling, P.J., Parsons, D.R., Sumner, E.J., Clare, M.A., Simmons,
283   S.M., Cooper, C., and Pope, E.L., 2017b, Newly recognized turbidity current structure can explain
284   prolonged flushing of submarine canyons: Science advances, v. 3, p. e1700200,
285   doi:10.1126/sciadv.1700200.

286 Baas, J.H., Van Kesteren, W., and Postma, G., 2004, Deposits of depletive high-density turbidity currents:
287   a flume analogue of bed geometry, structure and texture: Sedimentology, v. 51, p. 1053–1088,
288   doi:10.1111/j.1365-3091.2004.00660.x.

289 Babonneau, N., Savoye, B., Cremer, M., and Bez, M., 2010, Sedimentary Architecture in Meanders of a
290   Submarine Channel: Detailed Study of the Present Congo Turbidite Channel (Zaiango Project):
291   Journal of Sedimentary Research, v. 80, p. 852–866, doi:10.2110/jsr.2010.078.

292 Bagnold, R.A., 1966, An Approach to the Sediment Transport Problem from General Physics: U.S.
293   Government Printing Office

294 Cantelli, A., Pirmez, C., Johnson, S., and Parker, G., 2011, Morphodynamic and Stratigraphic Evolution
295   of Self-Channelized Subaqueous Fans Emplaced by Turbidity Currents: Journal of Sedimentary
296   Research, v. 81, p. 233–247, doi:10.2110/jsr.2011.20.

297 Cartigny, M.J.B., Eggenhuisen, J.T., Hansen, E.W.M., and Postma, G., 2013, Concentration-dependent
298   flow stratification in experimental high-density turbidity currents and their relevance to turbidite
299   facies models: Journal of Sedimentary Research, v. 83, p. 1047–1065

300 Conway, K.W., Barrie, J.V., Picard, K., and Bornhold, B.D., 2012, Submarine channel evolution: active
301   channels in fjords, British Columbia, Canada: Geo-Marine Letters, v. 32, p. 301–312,
302   doi:10.1007/s00367-012-0280-4.

303 Edmonds, D.A., Shaw, J.B., and Mohrig, D., 2011, Topset-dominated deltas: A new model for river delta
304   stratigraphy: Geology.

305 Eggenhuisen, J.T., and McCaffrey, W.D., 2012, The vertical turbulence structure of experimental
306   turbidity currents encountering basal obstructions: implications for vertical suspended sediment
307   distribution in non-equilibrium currents: Sedimentology, v. 59, p. 1101–1120, doi:10.1111/j.1365-
308   3091.2011.01297.x.

309 Eggenhuisen, J.T., McCaffrey, W.D., Haughton, P.D.W., and Butler, R.W.H., 2010, Small-Scale Spatial
310   Variability in Turbidity-Current Flow Controlled by Roughness Resulting from Substrate Erosion:
311   Field Evidence for a Feedback Mechanism: Journal of Sedimentary Research, v. 80, p. 129–136,
312   doi:10.2110/jsr.2010.014.

313 Fernandes, A.M., Mohrig, D., and Buttles, J., 2018, A New Mechanism for Terrace Formation in
314   Submarine Canyons: EarthArXiv. September, v. 1, doi: 10.31223/osf.io/a6p7y

315 Garcia, M.H., 2008, Sedimentation Engineering: Theories, Measurements, Modeling and Practice:
316   Processes, Management, Modeling, and Practice (Asce Manual and Reports on Engineering Practice
317   No: American Society of Civil Engineers.

318 Garcia, M., and Parker, G., 1989, Experiments on hydraulic jumps in turbidity currents near a canyon-fan
319   transition: Science, v. 245, p. 393–396, doi:10.1126/science.245.4916.393.

320 Howard, A.D., 1994, A detachment-limited model of drainage basin evolution: Water resources research,
321   v. 30, p. 2261–2285, doi:10.1029/94WR00757.

322 Howard, A.D., 1980, Thresholds in river regimes: Thresholds in geomorphology, p. 227–258.

323 Hughes Clarke, J.E., 2016, First wide-angle view of channelized turbidity currents links migrating cyclic
324   steps to flow characteristics: Nature communications, v. 7, p. 11896, doi:10.1038/ncomms11896.

325 Janocko, M., Cartigny, M.B.J., Nemec, W., and Hansen, E.W.M., 2013, Turbidity current hydraulics and
326   sediment deposition in erodible sinuous channels: Laboratory experiments and numerical
327   simulations: Marine and Petroleum Geology, v. 41, p. 222–249,
328   doi:10.1016/j.marpetgeo.2012.08.012.

329 Johnson, J.P., and Whipple, K.X., 2007, Feedbacks between erosion and sediment transport in
330   experimental bedrock channels: Earth Surface Processes and Landforms, v. 32, p. 1048–1062,
331   doi:10.1002/esp.1471.

332 Johnson, J.P.L., Whipple, K.X., Sklar, L.S., and Hanks, T.C., 2009, Transport slopes, sediment cover, and
333   bedrock channel incision in the Henry Mountains, Utah: Journal of geophysical research, v. 114, p.
334   W12446, doi:10.1029/2007JF000862.

335 Kane, I.A., McCaffrey, W.D., and Peakall, J., 2008, Controls on sinuosity evolution within submarine

336   channels: Geology, v. 36, p. 287–290, doi:10.1130/G24588A.1.

337   Khripounoff, A., Vangriesheim, A., Babonneau, N., Crassous, P., Dennielou, B., and Savoye, B., 2003,
338   Direct observation of intense turbidity current activity in the Zaire submarine valley at 4000 m water
339   depth: Marine geology, v. 194, p. 151–158, doi:10.1016/S0025-3227(02)00677-1.

340   Leeder, M.R., and Bridges, P.H., 1975, Flow separation in meander bends: Nature, v. 253, p. 338,
341   doi:10.1038/253338a0.

342   de Leeuw, J., Eggenhuisen, J.T., and Cartigny, M.J.B., 2016, Morphodynamics of submarine channel
343   inception revealed by new experimental approach: Nature communications, v. 7, p. 10886,
344   doi:10.1038/ncomms10886.

345   Luthi, S. an, 1981, Experiments on non-channelized turbidity currents and their deposits: Marine geology,
346   v. 40, p. M59–M68, doi:10.1016/0025-3227(81)90139-0.

347   Métivier, F., Lajeunesse, E., and Cacas, M.-C., 2005, Submarine Canyons in the Bathtub: Journal of
348   Sedimentary Research, v. 75, p. 6–11, doi:10.2110/jsr.2005.002.

349   Middleton, G.V., 1966, Small-scale models of turbidity currents and the criterion for auto-suspension:
350   Journal of Sedimentary Research, v. 36, p. 202–208, doi:10.1306/74D71442-2B21-11D7-
351   8648000102C1865D.

352   Mitchell, N.C., 2014, Bedrock erosion by sedimentary flows in submarine canyons: Geosphere, v. 10, p.
353   892–904, doi:10.1130/GES01008.1.

354   Mohrig, D., and Buttles, J., 2007, Deep turbidity currents in shallow channels: Geology, v. 35, p. 155–
355   158, doi:10.1130/G22716A.1.

356   Nino, Y., Lopez, F., and Garcia, M., 2003, Threshold for particle entrainment into suspension:
357   Sedimentology, v. 50, p. 247–263, doi:10.1046/j.1365-3091.2003.00551.x.

358   Nittrouer, J.A., Mohrig, D., and Allison, M., 2011a, Punctuated sand transport in the lowermost
359   Mississippi River: Journal of geophysical research, v. 116, p. F04025, doi:10.1029/2011JF002026.

360   Nittrouer, J.A., Mohrig, D., Allison, M.A., and Peyret, A.-P.B., 2011b, The lowermost Mississippi River:
361   a mixed bedrock-alluvial channel: Sedimentology, v. 58, p. 1914–1934, doi:10.1111/j.1365-
362   3091.2011.01245.x.

363   Pirmez, C., Beaubouef, R.T., Friedmann, S.J., and Mohrig, D.C., 2000, Equilibrium profile and baselevel
364   in submarine channels: examples from Late Pleistocene systems and implications for the architecture
365   of deepwater reservoirs, *in* Global deep-water reservoirs: Gulf Coast Section SEPM Foundation 20th
366   Annual Bob F. Perkins Research Conference, p. 782–805.

367   Rowland, J.C., Hilley, G.E., and Fildani, A., 2010, A Test of Initiation of Submarine Leveed Channels by
368   Deposition Alone: Journal of Sedimentary Research, v. 80, p. 710–727, doi:10.2110/jsr.2010.067.

369   Shepherd, R.G., and Schumm, S.A., 1974, Experimental Study of River Incision: GSA Bulletin, v. 85, p.
370   257–268, doi:2.0.CO;2">10.1130/0016-7606(1974)85<257:ESORI>2.0.CO;2.

371   Shields, A., 1936, Anwendung der Aehnlichkeitsmechanik und der Turbulenzforschung auf die
372   Geschiebebewegung: PhD Thesis Technical University Berlin.

373 Sklar, L.S., and Dietrich, W.E., 2004, A mechanistic model for river incision into bedrock by saltating
374   bed load: Water resources research, v. 40, doi: 10.1029/2003WR002496.

375 Smith, J.D., and Hopkins, T.S., 1971, Sediment Transport on the Continental Shelf Off of Washington
376   and Oregon in Light of Recent Current Measurements: Washington Univ., Seattle. Dept. of
377   Oceanography. Atomic Energy Commission, U. S. A.

378 Straub, K.M., Mohrig, D., Buttles, J., McElroy, B., and Pirmez, C., 2011, Quantifying the influence of
379   channel sinuosity on the depositional mechanics of channelized turbidity currents: A laboratory
380   study: Marine and Petroleum Geology, v. 28, p. 744–760, doi:10.1016/j.marpetgeo.2010.05.014.

381 Straub, K.M., Mohrig, D., McElroy, B., and Buttles, J., 2008, Interactions between turbidity currents and
382   topography in aggrading sinuous submarine channels: A laboratory study: GSA Bulletin today: a
383   publication of the Geological Society of America, doi: 120/3-4/368/2260.

384 Symons, W.O., Sumner, E.J., Paull, C.K., Cartigny, M.J.B., Xu, J.P., Maier, K.L., Lorenson, T.D., and
385   Talling, P.J., 2017, A new model for turbidity current behavior based on integration of flow
386   monitoring and precision coring in a submarine canyon: Geology, v. 45, p. 367–370,
387   doi:10.1130/G38764.1.

388 Vachtman, D., Mitchell, N., and Gawthorpe, R., 2013, Morphologic signatures in submarine canyons and
389   gullies, central USA Atlantic continental margins: v. 41, p. 250–263,
390   doi:10.1016/j.marpetgeo.2012.02.005.

391 van Rijn Leo C., 1984, Sediment Transport, Part III: Bed forms and Alluvial Roughness: Journal of
392   Hydraulic Engineering, v. 110, p. 1733–1754, doi:10.1061/(ASCE)0733-9429(1984)110:12(1733).

393 Weill, P., Lajeunesse, E., Devauchelle, O., Métiver, F., Limare, A., Chauveau, B., and Mouazé, D., 2014,
394   Experimental investigation on self-channelized erosive gravity currents: Journal of Sedimentary
395   Research, v. 84, p. 487–498. Doi: 84/6/487/145405.

396 Whipple, K.X., 2004, Bedrock Rivers and the Geomorphology of Active Orogens: Annual review of earth
397   and planetary sciences, v. 32, p. 151–185, doi:10.1146/annurev.earth.32.101802.120356.

398 Whipple, K.X., Hancock, G.S., and Anderson, R.S., 2000, River incision into bedrock: Mechanics and
399   relative efficacy of plucking, abrasion, and cavitation: GSA Bulletin, v. 112, p. 490–503,
400   doi:2.0.CO;2">10.1130/0016-7606(2000)112<490:RIIBMA>2.0.CO;2.

401 Xu, J.P., 2010, Normalized velocity profiles of field-measured turbidity currents: Geology, v. 38, p. 563–
402   566, doi:10.1130/G30582.1.

403 Xu, J.P., Barry, J.P., and Paull, C.K., 2013, Small-scale turbidity currents in a big submarine canyon:
404   Geology, v. 41, p. 143–146, doi:10.1130/G33727.1.

405 Xu, J.P., Noble, M.A., and Rosenfeld, L.K., 2004, In-situ measurements of velocity structure within
406   turbidity currents: Geophysical research letters, v. 31, doi:10.1029/2004GL019718.

407 Yu, B., Cantelli, A., Marr, J., Pirmez, C., O'Byrne, C., and Parker, G., 2006, Experiments on Self-
408   Channelized Subaqueous Fans Emplaced by Turbidity Currents and Dilute Mudflows: Journal of
409   Sedimentary Research, v. 76, p. 889–902, doi:10.2110/jsr.2006.069.

410

411   **Figures and captions:**

412

413
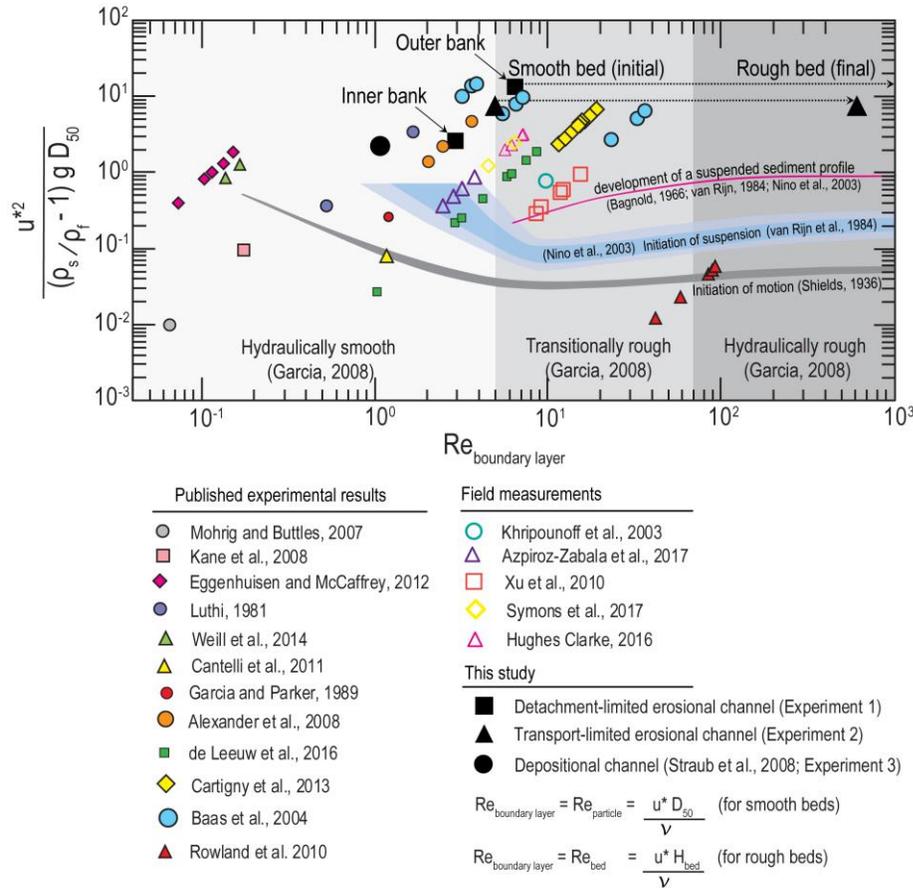
428

429   Figure 2: The modified Shield's scaling approach of de Leeuw et al., 2016, used here to compare our

430   experiments to various experimental and field studies. Note that the initial conditions in all 3 experiments

431   presented in this study span the threshold between hydraulically smooth and transitionally rough flow.

432   Bed roughness that evolved in Experiments 1 and 2 increased the turbulence in the boundary, causing it to

433   become hydraulically rough. (Luthi, 1981; Garcia and Parker, 1989; Khripounoff et al., 2003; Baas et al.,

434   2004; Mohrig and Buttles, 2007; Alexander et al., 2007; Straub et al., 2008; Kane et al., 2008; Xu, 2010;

435   Rowland et al., 2010; Cantelli et al., 2011; Eggenhuisen and McCaffrey, 2012; Cartigny et al., 2013;

436   Weill et al., 2014; de Leeuw et al., 2016; Hughes Clarke, 2016; Symons et al., 2017; Azpiroz-Zabala et

437   al., 2017b). Hydraulic thresholds based on (Shields, 1936; Bagnold, 1966; van Rijn Leo C., 1984; Nino et

438   al., 2003; Garcia, 2008)
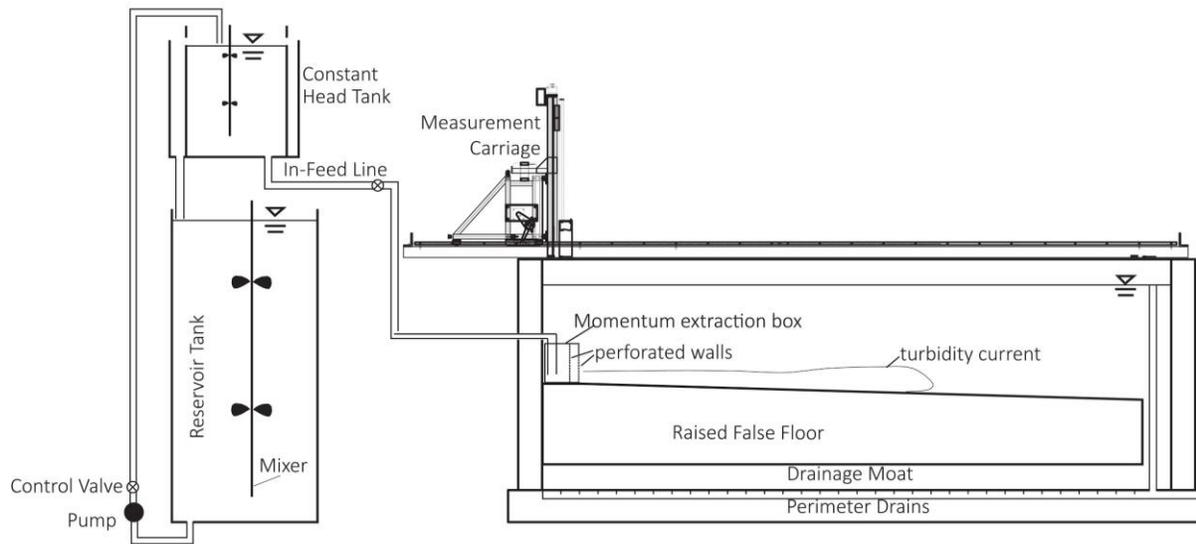
439

440   Figure 2: A generalized schematic of the experimental basin set-up used for the three experiments.

441
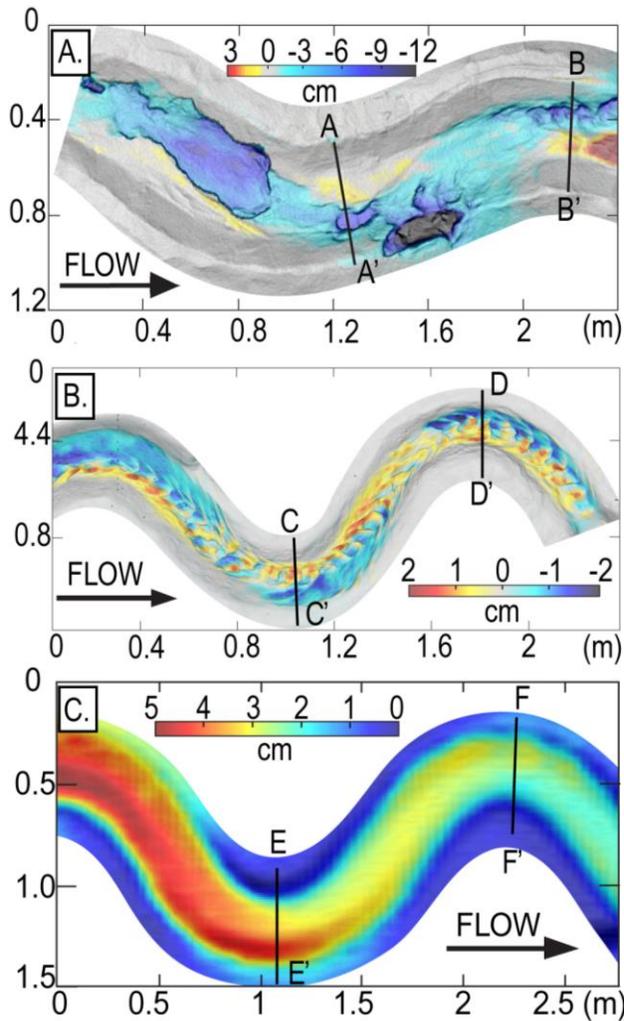
Figure 3: Difference maps defining net elevation change in all three experiments.. (A) Detachment-limited erosion in Experiment 1 resulted in a rough bed patterned with erosional bedforms along a semi-continuous erosional inner channel that followed the path of the high velocity core, and terraces formed at inner banks. (B) Transport-limited erosion in Experiment 2 resulted in a semi-continuous mobile sediment bed, reworked into ripples. (C) Consistent deposition in Experiment 3 resulted in a channel that was persistently aggradational, with the thickest deposits at the outsides of bends.

456
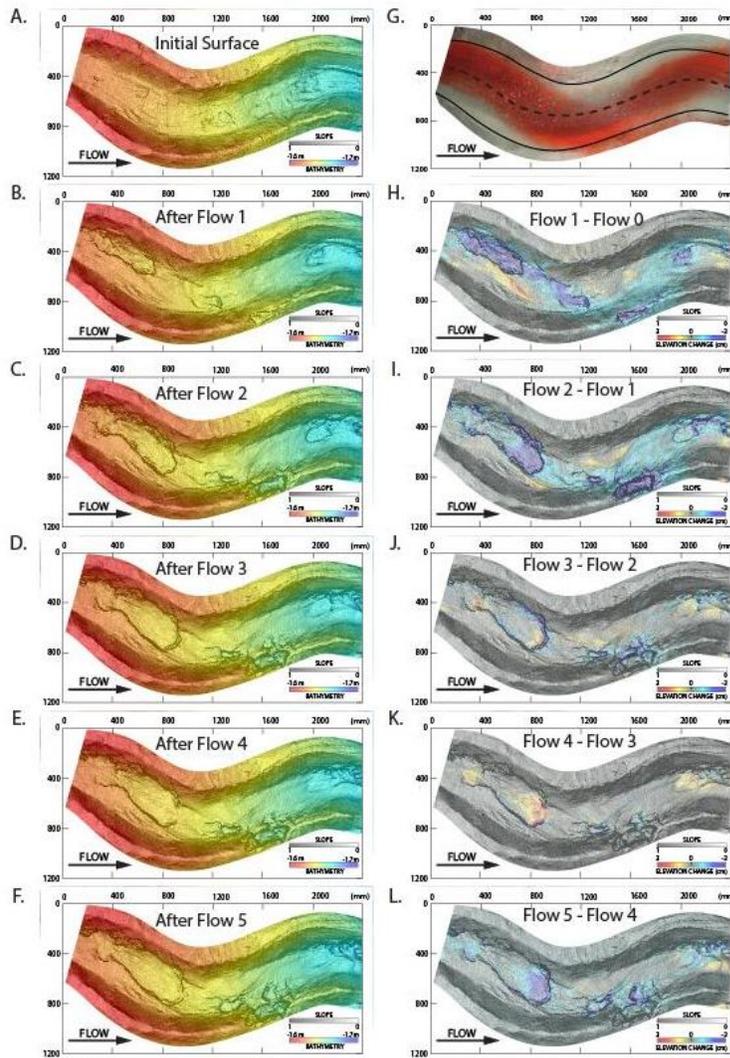
Figure 4: (A-F) Experiment 1 time-lapse laser-scanned topographic maps showing how the 5 experimental currents evolved the experimental channel. (G) Orthorectified overhead photograph showing the pathway of the high velocity core of the current- tracked by red dye with the most intensity. The very small amounts of red dye near the inner banks bear testament to very low velocities in these zones. (H-L) is a series of difference maps that define patterns of erosion and deposition within the experimental channel due to the passage of the 5 density currents. Note how erosion (cold colors) tracks the pathway of the high velocity core (intense red dye in G) and no erosion weak deposition (warm colors) is associated with inner bank zones visited by separated flow (low amount of red dye in G).

476

477

478
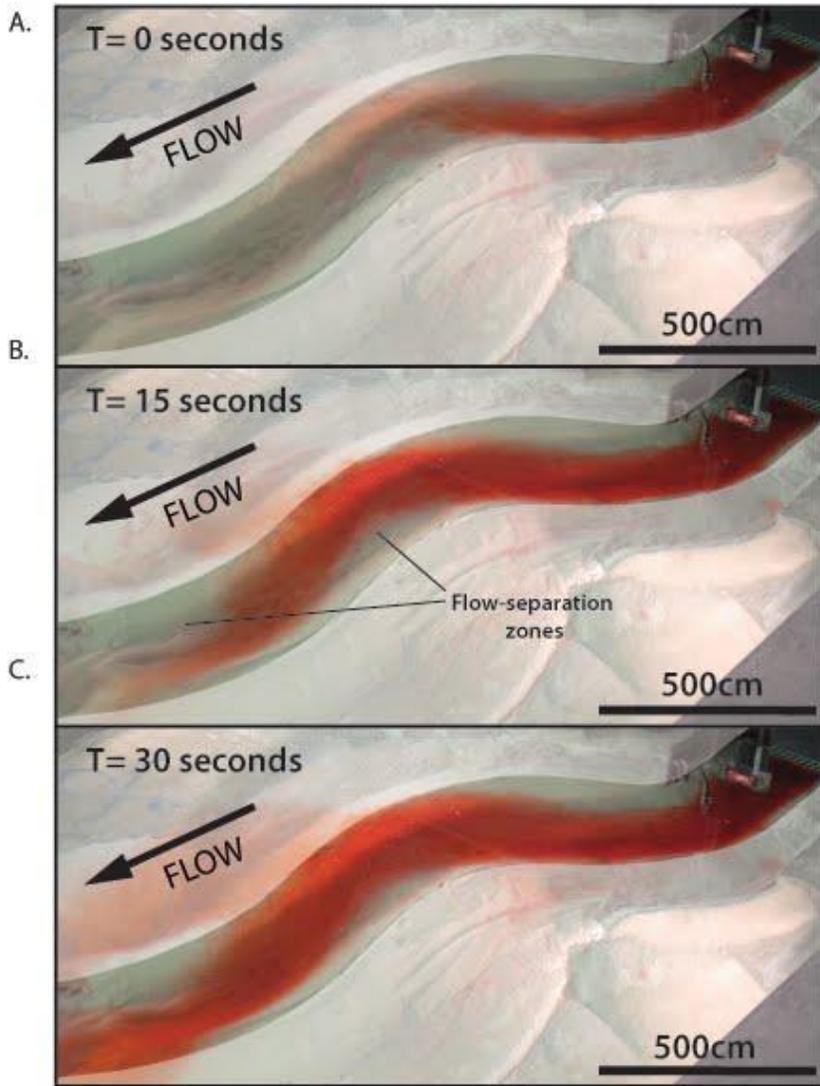
Figure 5: A-C Time lapse photographs showing a pulse of red dye in the current that defines the pathway of the high-velocity core of the current. Low velocity zones where flow separated from the inner banks received the dyed current later than the outside of bends and the dye intensity was always lower than at the outside of bends.

496

497

498
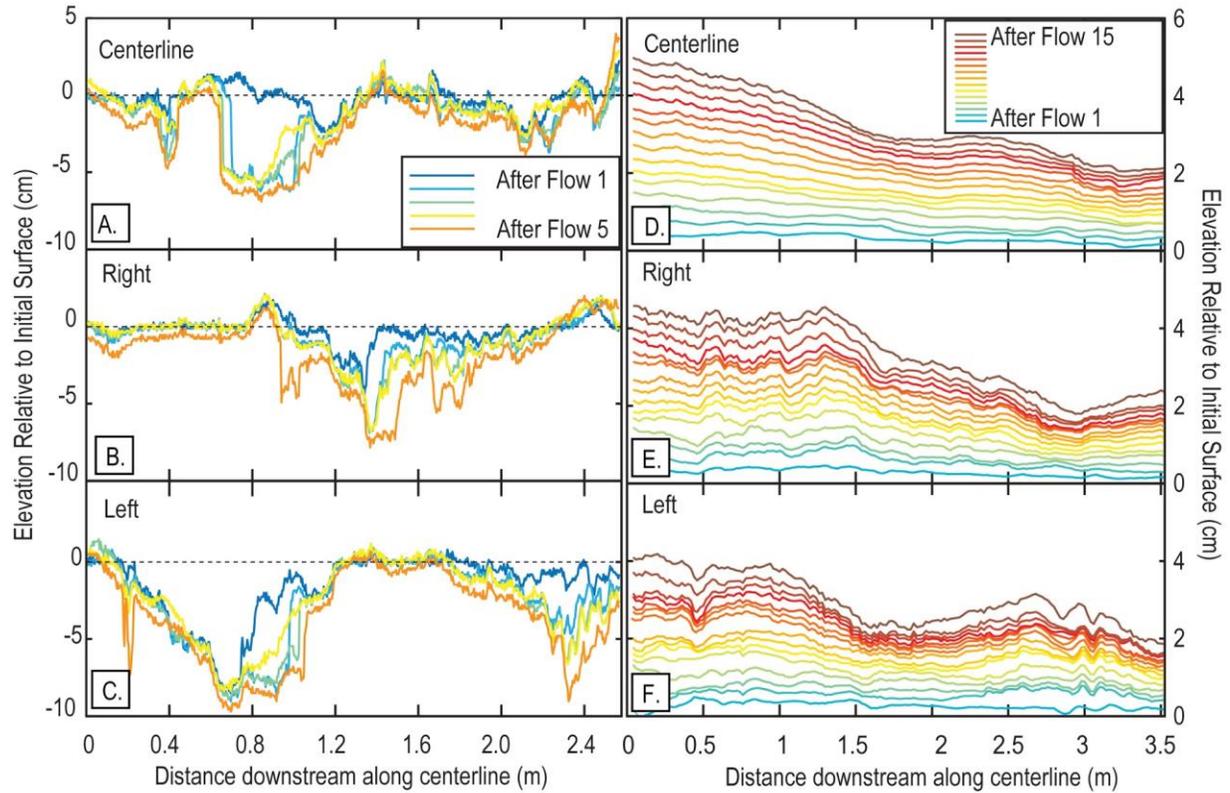
Figure 6: A-C) Change in elevation of the channel bed in Experiment 1 after the passage of 5 consecutive flows, along (A) the centerline, (B) 15 cm right of the centerline, and (C) 15 cm left of the centerline. D-F) Change in elevation of the channel bed in Experiment 3 after the passage of 15 consecutive flows, along (A) the centerline, (B) 5 cm right of the centerline, and (C) 5 cm left of the centerline.
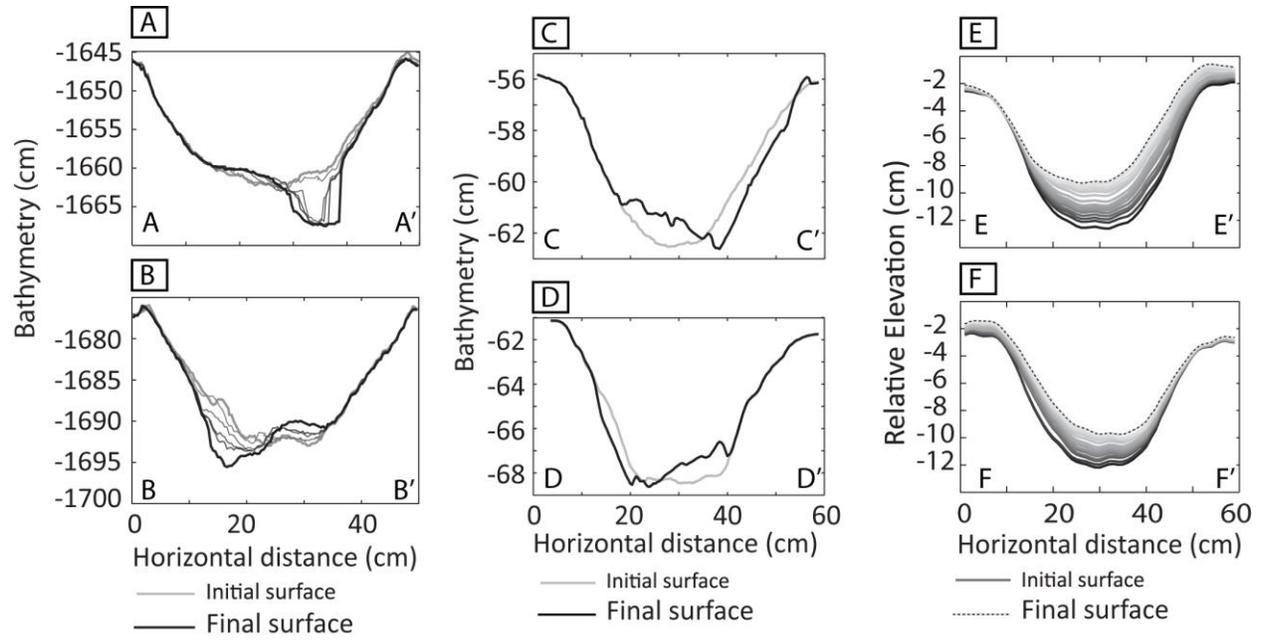
507

508 Figure 7: Cross sections showing time-lapse topographic evolution at the apices of the second and third
509 bends in Experiment 1 (A-B), Experiment 2 (C-D) and Experiment 3 (E-F).